AGU PUBLICATIONS

JGR

Journal of Geophysical Research: Solid Earth

RESEARCH ARTICLE
10.1002/2015JB011897

Key Points:
- Etna LP activity behavior is compared with tectonic earthquakes recurrence laws
- Similarity in recurrence distributions of Etna and Stromboli LP activities
- LP source at Etna is consistent with a degassing process occurring at depth

Supporting Information:
- Figures S1–S6

Correspondence to:
L. Cauchie,
lena.cauchie@ingv.it

Citation:
Cauchie, L., G. Saccorotti, and C. J. Bean (2015), Amplitude and recurrence time analysis of LP activity at Mount Etna, Italy, *J. Geophys. Res. Solid Earth*, *120*, 6474–6486, doi:10.1002/2015JB011897.

Received 21 JAN 2015
Accepted 10 AUG 2015
Accepted article online 14 AUG 2015
Published online 24 SEP 2015

Amplitude and recurrence time analysis of LP activity at Mount Etna, Italy

Léna Cauchie[1,2], Gilberto Saccorotti[1], and Christopher J. Bean[2,3]

[1]Istituto Nazionale di Geofisica e Vulcanologia, Pisa, Italy, [2]School of Geological Sciences, University College Dublin, Dublin, Ireland, [3]Geophysics Section, School of Cosmic Physics, Dublin Institute for Advanced Studies, Dublin, Ireland

Abstract The aim of this work is to improve our understanding of the long-period (LP) source mechanism at Mount Etna (Italy) through a statistical analysis of detailed LP catalogues. The behavior of LP activity is compared with the empirical laws governing earthquake recurrence, in order to investigate whether any relationships exist between these two apparently different earthquake classes. We analyzed a family of 8894 events detected during a temporary experiment in August 2005. For that time interval, the LP activity is sustained in time and the volcano did not exhibit any evident sign of unrest. The completeness threshold of the catalogue is established through a detection test based on synthetic waveforms. The retrieved amplitude distribution differs significantly from the Gutenberg-Richter law, and the interevent times distribution does not follow the typical γ law, expected for tectonic activity. In order to compare these results with a catalogue for which the source mechanism is well established, we applied the same procedure to a data set from Stromboli Volcano, where recurrent LP activity is closely related to very-long-period pulses, in turn associated with the summit explosions. Our results indicate that the two catalogues exhibit similar behavior in terms of amplitude and interevent time distributions. This suggests that the Etna's LP signals are most likely driven by stress changes caused by an intermittent degassing process occurring at depth, similar to that which drives the summit explosions at Stromboli Volcano.

1. Introduction

Long-period (LP) seismic activity is observed at many volcanoes worldwide, and its manifestation is different depending on the particular volcanic context taken into account. The LP source mechanism is generally associated with the resonance of fluid-filled cavities like cracks or conduits [*Chouet*, 1985, 1986]. In such models, the marked impedance contrast at the fluid-rock interface would induce the establishment of interface waves whose frequencies are significantly lower than those expected on the basis of both the dimension of the resonator and the acoustic velocity of the fluid contained therein [e.g., *Aki et al*., 1977; *Chouet*, 1985, 1986, 1988, 1992; *Fujita et al*., 1995; *Chouet*, 1996; *Kumagai and Chouet*, 2001; *Neuberg*, 2000; *Neuberg et al*., 2000; *Kumagai et al*., 2002]. The mechanism triggering the resonance, however, is still not fully understood. Thus far, models addressing the excitation of the resonator include instabilities in the fluids as acoustic emissions of collapsing bubbles, sudden pressure drop caused by unsteady chocked flow, and discharge of fluid from the resonator, thus generating the LP waveform [e.g., *Nakano et al*., 2003; *Arciniega-Ceballos et al*., 2003; *Chouet*, 1992, 1996; *Kumagai et al*., 2005]. Additional trigger models are instead based on the brittle failure of a high viscous magma in the glass transition [*Tuffen et al*., 2003; *Neuberg et al*., 2006].

Based on a lack of LP resonance when observed in the near field, an alternative model for LP genesis has been recently proposed by *Bean et al*. [2014], who used numerical simulations to show that slow-rupture failure in unconsolidated volcanic materials can reproduce all key aspects of LP observations. Therefore, *Bean et al*. [2014] suggested that LP signals might not be direct indicators of fluid-rock interaction; rather, they could represent a marker of deformation in the upper volcanic edifice associated with stress changes driven by volcanic processes and/or gravitational instability. Under that perspective, LP spectra would lie in between slow-slip earthquakes and fast dynamic rupture.

Recently, LP sources at a number of volcanoes worldwide have been extensively studied using full-waveform moment tensor (MT) inversion [e.g., *Nakano et al*., 2003; *Lokmer et al*., 2007; *Aster et al*., 2008; *Davi et al*., 2010; *De Barros et al*., 2011]. For the particular case of Mount Etna, *Lokmer et al*. [2007] and *De Barros et al*. [2011] applied estimated crack-like geometries for the LP sources observed throughout the 2004–2008 time span.

Topography, velocity model, and location of the events are important aspects in the moment tensor inversion. Indeed, *Bean et al*. [2008] and *Cesca et al*. [2008] showed that a poor knowledge of the velocity structure can lead to apparently stable but spurious solutions. Furthermore, the emergent onset that characterize LP events and the highly heterogeneous media usually encountered in volcanic environment render LP events difficult to locate.

In a companion paper (L. Cauchie et al., Uncertainties in source location and mechanism at Etna Volcano, Italy, submitted to *Journal of Volcanology and Geothermal Research*, hereinafter referred to as P1, 2014) we highlight that a mislocation of the LP source may lead to an erroneous estimate of the force system as derived from MT inversion. In general, a reliable estimate of the source parameters relies on dense network coverage and accurate knowledge of the velocity structure, two factors which are only rarely achieved.

Here we present an alternative study of the LP events features aimed at the understanding of their origin. We exploit the sustained character of LP activity to present an analysis of the interevent time and amplitude distributions of a complete catalogue of LP events detected at Mount Etna in August 2005. The behavior of the LP activity is compared with the empirical laws governing earthquake recurrence (e.g., Gutenberg-Richter and γ law distributions), in order to understand the relationships between these apparently two different classes of sources.

The investigation of large catalogues of events is a useful tool to understand the behavior of volcano seismicity with respect to tectonic environments [*Traversa and Grasso*, 2010; *Matoza and Chouet*, 2010].

In particular, we analyzed a catalogue of 8894 events detected in August 2005 which is described in the companion paper (P1). The completeness of the catalogue is assessed through the application of a detection test presented in this work. The retrieved amplitude and interevent time distributions differ significantly from the Gutenberg-Richter and γ law. In order to compare these results with a catalogue for which the source mechanism is well established, we applied the same procedure to a data set from Stromboli Volcano, where broadband seismic signals are associated with the recurrent summit explosions [e.g., *Ripepe et al*., 1993; *Neuberg et al*., 1994; *Neuberg and Luckett*, 1996; *Chouet et al*., 1999]. The explosion signals at Stromboli exhibit similar amplitude and interevent time distributions with respect to those observed for LP activity at Mount Etna. However, Mount Etna does not exhibit similar explosive activity to Stromboli. Hence, this suggests that a plausible interpretation of the Etna's LP data is a process driven by stress changes related to an intermittent degassing, occurring at depth.

2. Instruments and Data

Data used for this study were gathered during several seismic experiments conducted at Etna and Stromboli Volcanoes in 2005 and 2011, respectively. At Etna Volcano, the data set is composed of records of three seismic stations installed on the summit of the volcano (ET00, ET01, and ET29 in Figure 1a). These three stations are part of a sparse network of nine Lennartz three-component seismometers with flat frequency response down to 0.05 Hz and with a sampling rate of 125 samples per second. We also analyzed data from a small array located on the south flank of the volcano (ACPN in Figure 1a). It was composed of six Lennartz LE3D-lite seismometers with a flat response down to 1 Hz and sampling rate of 125 samples per second. For the purpose of this work, we used 1 month of continuous recordings spanning the 1–31 August 2005 time interval; before the analysis, data were corrected for the instrument response. The Stromboli data set consists of recordings from four seismic stations belonging to the permanent seismic network monitoring the activity of the volcano. The instruments are Guralp CMG-40T with flat amplitude response down to 0.016 Hz and sampling rate of 50 samples per second. For this study, we analyzed 1 month of data from 1 to 31 July 2011. The locations of the seismic stations are represented in Figure 1b.

3. Amplitude and Interevent Times Distributions of Long-Period Activity at Mount Etna

Throughout the period of our observations, LP activity at Etna was sustained over time with rates of hundreds of events per day. The events were first detected by a Short-Term/Long-Term Average ratio approach (STA/LTA) [*Earle and Shearer*, 1994] applied over 0.3 Hz–1 Hz band-pass filtered signals recorded at the three summit stations and the central station of the array ACPN (see Figure 1). In order to avoid local transients, only

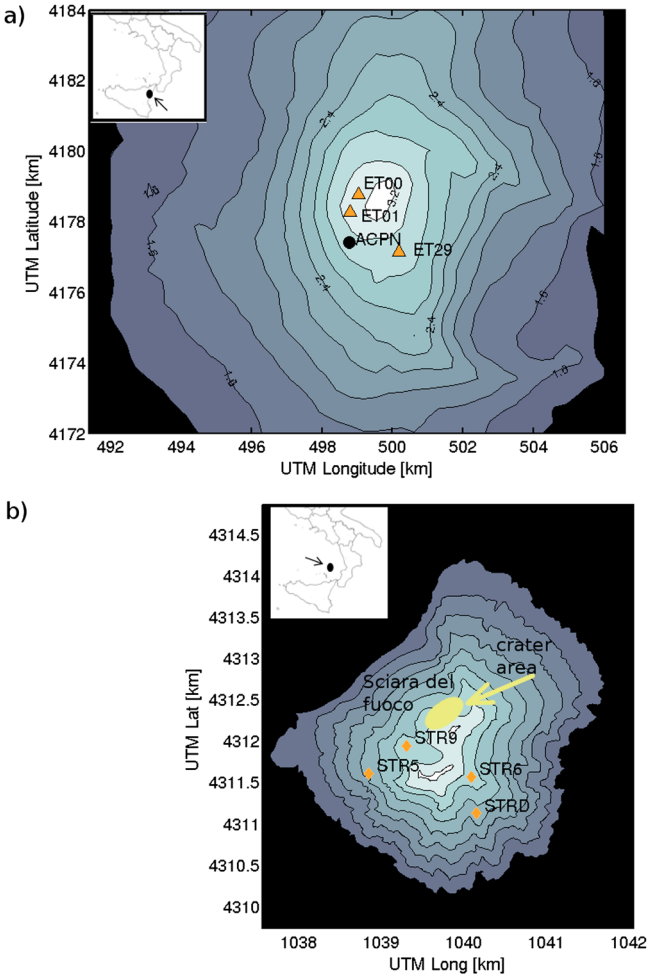

Figure 1. Location and geometry of the seismic networks deployed on (a) Mount Etna and (b) Stromboli Volcano.

the events which triggered at least three stations were taken into account. In August 2005, this first catalogue amounts to 12795 events. Because of the high degree of similarity observed among the events (see Figures S1 and S2 in the supporting information), we performed a cross-correlation analysis and classified them into two main families exhibiting similar waveforms. The richness of these two catalogues was further improved through application of a match filtering procedure applied to data from station ET00. This procedure consists in sliding sample-by-sample a template wavelet along the continuous data streams. At each time step, a correlation coefficient is computed between the template wavelet and the corresponding window of the continuous recording. If the correlation coefficient is greater than a given threshold (0.8 in our case), an event is declared. The template wavelets were obtained by stacking the aligned seismograms pertaining to individual families. The two families of events thus retrieved differ in size, spectral content, and location (see Figure S3 in the supporting information).

Out of these two families, in the present work we focus on the richest one (8894 detections; hereinafter referred to as Family 1), which is characterized by the largest amplitudes. Indeed, the amplitudes of the second family of events are lower than the average noise level, which has been estimated by averaging the absolute amplitudes measured over 5 s long time windows preceding each LP signal. The noise level is reported in Figure 3a with the black vertical line. These events are located below the crater area (Universal Transverse Mercator 499.1, 4178.2 km) and are distributed between the surface and about 1 km depth (see Figure S4 in the supporting information). For this catalogue, typical LP waveforms at station ET00 (epicentral distance ~1 km) are characterized by emergent onset and a duration of about 10 s, with a dominant frequency around 0.5 Hz (Figure 2).

Amplitudes of individual events are calculated by averaging the absolute values of the vertical component seismograms over 14 s long windows encompassing the maximum peak-to-peak displacement at station ET00. Figure S5 shows the evident linear scaling between the amplitudes measured on the vertical component and those obtained from the modulus of the 3C vector of ground motion. Such equivalence suggests that the energy partition between different ground motion components (i.e., radiation pattern) remains stable throughout the observation period, and for different event size.

A further issue concerns the bias in single-station estimate of the source amplitude if the location of the source varies in time. On the one hand, waveform similarity suggests that the spatial spreading of LP sources should be at maximum on the order of 500–1000 m (i.e., a quarter of the dominant wavelength). On the other hand, the near-field conditions of our measurements imply that even tight changes of the source-to-station distance reflect into dramatic variations of the observed amplitudes. In the companion paper, we discussed extensively all the uncertainties associated with different location procedures, showing the impossibility of

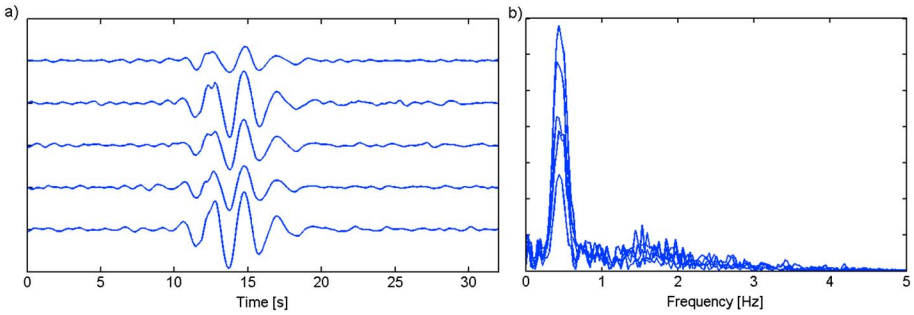

Figure 2. Characteristics of the Family I events detected on Mount Etna in August 2005: (a) Sample events extracted randomly in the catalogue; (b) associated amplitude spectra of the LP events in Figure 2a.

retrieving source positions with accuracies better than ~250 m and ~500 m along the two horizontal and vertical directions, respectively (see also Figure S4 in the supporting information). As a consequence, it is difficult to assess precisely the extent of the volume spanned by our LP Family I sources, and the consequent amplitude changes due to variable path lengths. In order to assess this issue, however, we tried to compare the amplitude distributions obtained at station ET00 with that derived at site ET29. Kolmogorov-Smirnov (KS) test indicates that the two different amplitude data sets are obtained by the same distribution (Figure S6 in the supporting information). In other words, our result would not change once accounting for data recorded by a different station, thus suggesting that the possible changes in path lengths associated with distinct source locations only have a second-order effect on the estimate of source amplitude.

These amplitudes are distributed following a unimodal distribution peaked at about 0.8×10^{-6} m (Figure 3a). Interevent times are computed as the time difference between events of index $(k+1)$ and k. The distribution of these differential times exhibits a peak at $t_c = 175 \pm 25$ s and an exponential decay for $t > t_c$ (Figure 3b). Figure 3c displays the relationship between the interevent times and the amplitudes of events of index $k+1$. No clear correlation exists between these two quantities: interevent times preceding the largest events are not necessarily longer than the repose times associated with events of smaller amplitudes.

3.1. Detection Test

Before proceeding with any statistical analysis of the distributions of LP amplitudes and interevent times, it is necessary to evaluate the completeness of our catalogue and to understand the limitations of our procedures. The determination of the completeness threshold of the catalogue will clarify if the small amount of LP events detected at small amplitudes is due to a limit of the detection procedures or if the generation of small amplitudes LP events is lower.

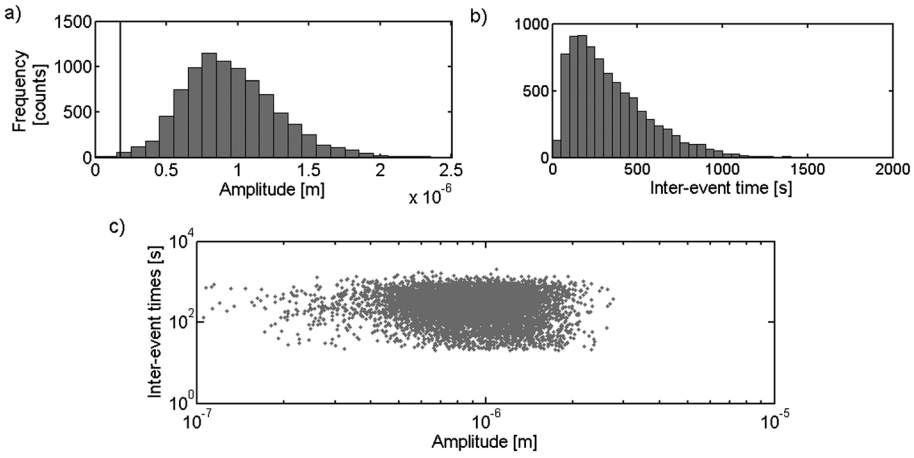

Figure 3. (a) Amplitude distribution of the LP events. The black vertical line in the amplitude histogram indicates the background noise level computed by averaging the absolute amplitudes over the 5 s long time windows preceding each LP event; (b) interevent time distribution; (c) amplitude versus interevent time behavior.

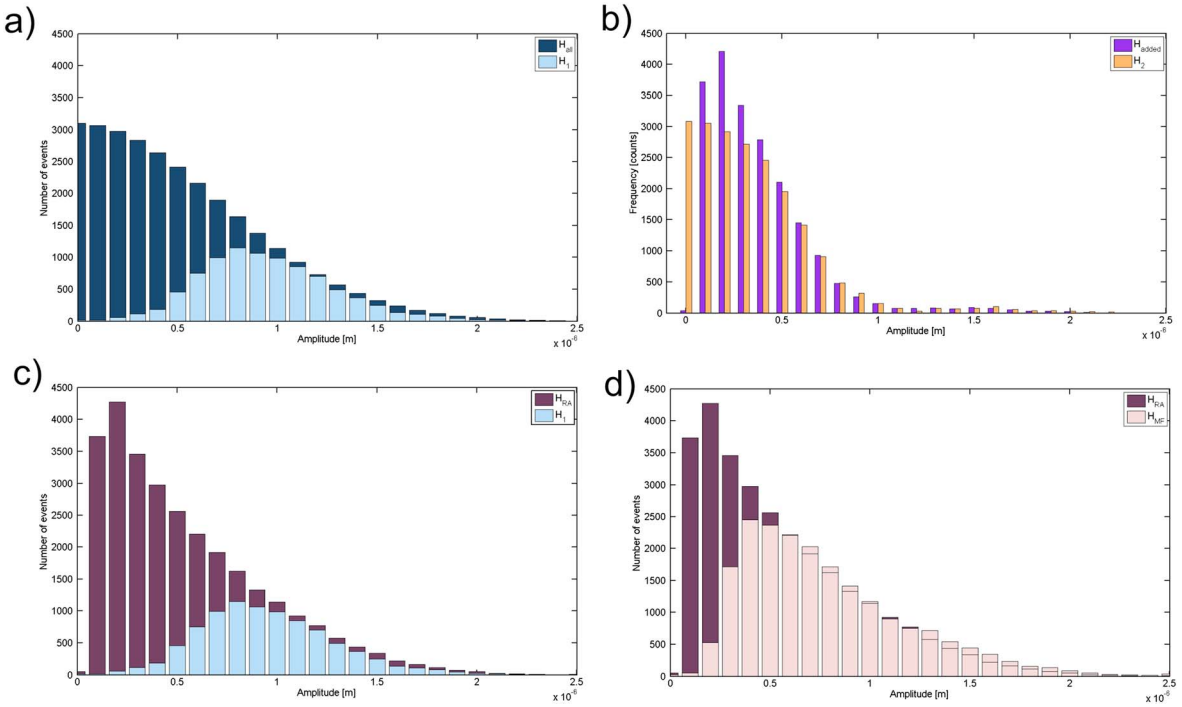

Figure 4. (a) Amplitude distribution of real LP events (H_1) and the new synthetic distribution (H_{all}); (b) amplitude distribution of added events (H_2) and correction for noise contribution H_{added}; (c) H_{RA}, the "known" amplitude distribution, is the sum between real detected events and added events amplitude distributions, compared to H_1; (d) measure amplitude distribution after application of the match filtering (H_{MF}) compared with H_{RA}.

We thus developed a detection test aimed at determining the robustness of catalogue construction via matched filtering. The method consists of repeating the matched filtering procedure over continuous data streams which have been enhanced by randomly inserting new synthetic LP events into the stream. The amplitudes of the synthetic LP events are decided to enrich the original distribution for the small amplitude bins.

The algorithm is structured according to the following steps:

1. We defined a new amplitude distribution H_{all} that enhances the contribution of small-amplitude events. This new distribution (Figure 4a) is defined as the sum of the observed histogram H_1 (computed from the real detected events) and a histogram (H_2) describing the amplitude distribution of synthetic events to be added.
2. We extracted randomly 200 waveforms from the true catalogue, to create a library of synthetic waveforms. These events are first filtered in the frequency range of interest (0.3–1 Hz) then replicated randomly in order to achieve the total number of events included in H_2. For each bin of H_{all}, the amplitudes of the corresponding number of synthetic events were randomly and uniformly scaled between the extreme values of that bin. This step is iterated for each amplitude bin.
3. The events are randomly distributed on a timescale and added to the real data stream, so forming the new traces. The distribution of the events over time satisfies the following restrictions: (i) two new, synthetic events cannot be superimposed: we set the minimum time interval between two consecutive events to 20 s; (ii) a new event cannot be superimposed to a real event previously detected by the match filter.
4. The insertion of the synthetic events onto the real recordings implies an increase of the amplitude of each event by an amount which is comparable to the average noise level. After their insertion into the real data streams, we thus measure the amplitudes of the synthetic events, deriving a corrected amplitude distribution H_{added} (see Figure 4b). While H_{added} and H_2 account for the same total number of events, the two distributions are markedly different (especially at low amplitudes) due to the effect of noise. H_{added} is eventually summed to H_1 to form the "true" amplitude distribution H_{RA} that accounts for the real and the synthetic added events (see Figure 4d).
5. We reprocess the new traces using the matched filter event detection. We finally calculate the amplitude distribution H_{MF} of this final catalogue and compare it to the known, synthetic histogram H_{RA}. In particular,

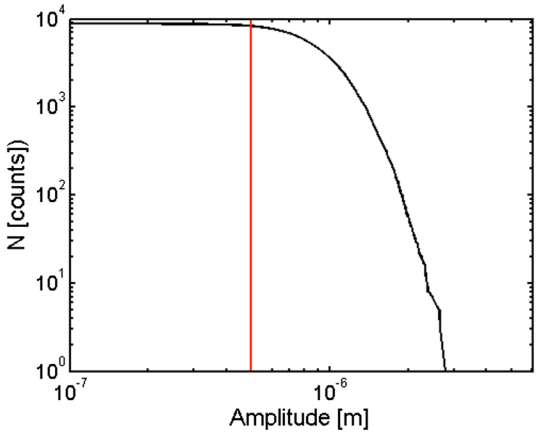

Figure 5. Black line: Cumulative amplitude distribution of the LP events; the red line represents the lower boundary of the complete catalogue.

we investigate if the number of events for each amplitude bin is retrieved (Figure 4d). The results in Figure 4d illustrate that the distribution H_{RA} is satisfactorily retrieved down to $A_d = 0.5 \times 10^{-6}$ m.

Below this threshold, the matched filter processing is not able to detect the events because of the poor signal-to-noise ratio.

This test suggests that all the events above A_d are detected, ensuring a complete catalogue on the amplitude range $[A_d, \rightarrow]$. The matched filter procedure implicitly assumes the action of a single source mechanism, radiating events of similar waveforms, as it is the case for the time period over which we investigate Mount Etna LPs.

3.2. Results With Completeness Threshold

For a catalogue of tectonic earthquakes, the relationship between the magnitudes M and total number of earthquakes is generally described by the Gutenberg-Richter (GR) law:

$$\log(N) = a - b \times M \tag{1}$$

In equation (1), N is the number of earthquakes whose magnitude is larger than or equal to M; a describes the overall event rate, and b—also termed the *b value*—measures the relative number of large quakes compared to the smaller ones. The b value is generally found to vary between 0.8 and 1.2 [*Shearer*, 2009] for a wide variety of regions and different magnitude scales. A tendency for the b value to decrease at small magnitudes is observed in the logarithmic version of the GR law, where the plot becomes flatter at the low magnitude end of the graph. This effect is due to the incompleteness of the catalogue due to the inadequate detection of smaller events.

For a given source-station pair, magnitude scales linearly with the logarithm of displacement amplitude A. Since our catalogue is associated with the radiation from a single source recorded by the same station, we analyzed our amplitude distribution using a modified version of equation (1):

$$\log(N) = a - b \times \log\ (A) \tag{2}$$

Figure 5 illustrates the cumulative amplitude distribution for our set of events. The completeness threshold is marked by a red line, corresponding to the A_d calculated using the detection test. For amplitudes greater than that threshold, the retrieved distribution does not exhibit the linear behavior which is predicted by the GR relationship. As this portion of the graph is representative of a complete catalogue of events, the possibility of a roll-off effect on the shape of the distribution is thus excluded in this case.

The analysis of interevent times can yield important clues for the understanding of the physical mechanisms driving the earthquake process. In various studies, the empirical interevent times distributions of tectonic activity were fitted by a γ law distribution [e.g., *Bak et al*., 2002; *Corral*, 2003, 2004]. A universal scaling law has then been proposed for the probability density function describing the interevent times, defined as the following γ distribution [*Corral*, 2003; *Traversa and Grasso*, 2010]:

$$P(\tau) = C\tau^{\gamma-1}e^{\frac{-\tau}{a}} \tag{3}$$

where $C = 0.5 \pm 0.1$, $\gamma = 0.67 \pm 0.05$, and $a = 1.58 \pm 0.15$. τ is the normalized interevent time obtained by multiplying the interevent time Δt by the average earthquake rate R.

In basaltic volcanic environments, *Traversa and Grasso* [2010] found that the interevent times of volcanotectonic events follow the law in equation (3) during quiet periods of activity, but not during eruptive episodes, when tectonic stresses are overwhelmed by those related to magmatic forcing.

Figure 6 shows the probability density function of seismic interevent times for the analyzed period of time and with reference to the complete part of the catalogue. We normalized the density distribution by the daily

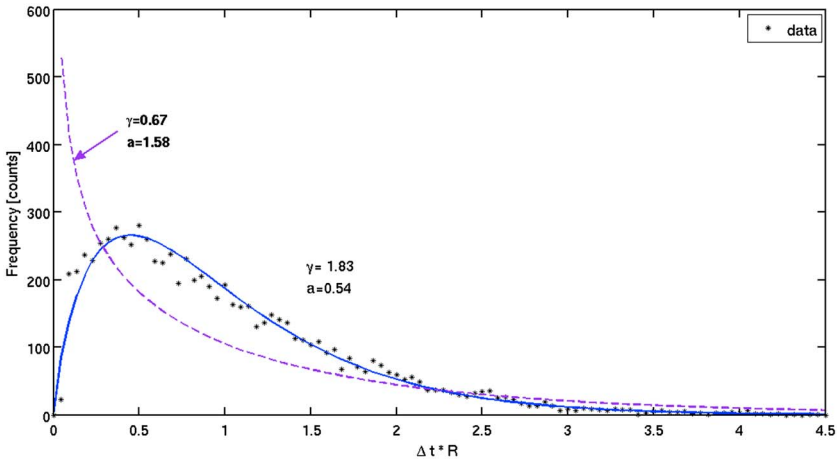

Figure 6. Interevent time distribution of LP events at Mount Etna fitted with a γ law of parameters $\gamma = 1.83$ and $a = 0.54$. The comparison with the γ law expected for tectonic activity ($\gamma = 0.67$; $a = 1.58$) is added.

event rate (286 in our case). We then compared this distribution with the γ law expected for the given range of repose times in equation (3). As we can observe in Figure 6, LP interevent times at Mount Etna deviate significantly from the theoretical distribution expected for tectonic seismicity (dashed line). The interevent times distributions do instead follow a γ law with the parameters $\gamma = 1.83$ and $a = 0.54$. The χ^2 test for the goodness-of-fit returns a p value = 0.3, buttressing the reliability of our estimates. The observation that the amplitude distributions do not follow the GR law and that the interevent times do not follow the same γ law as for typical tectonic activity indicates that the LP activity differs from typical tectonic earthquakes activity. This could either be controlled by edifice material conditions [*Bean et al.*, 2014], and/or stress state [*Traversa and Grasso*, 2010] and/or the mechanism acting at the source.

4. Explosive Activity at Stromboli Volcano

Located in the Tyrrhenian Sea off the southern coast of Italy, Stromboli Volcano (Figure 1) gives the name to the Strombolian activity that consists of mild, intermittent explosions occurring at a typical rate of 1–10 events per hour [*Blackburn et al.*, 1976]. Individual explosions are driven by large gas slugs that upon reaching the surface of the magma column cause the sudden release of gas that is accompanied by the ejection of molten lava fragments [*Blackburn et al.*, 1976]. Explosive vents are located inside a 350 × 150 m wide crater terrace at an elevation of about 750 m above sea level (asl) (see Figure 1 and *Rosi et al.* [2013]). Individual explosions are accompanied by broadband signals, whose energy spans the 0.05–10 Hz frequency band [*Neuberg et al.*, 1994; *Chouet et al.*, 1999]. Their typical duration is on the order of 40 s and the different waveforms are consistent with distinct explosion styles at the different craters [e.g., *Ripepe et al.*, 1993; *Neuberg et al.*, 1994; *Chouet et al.*, 2003]. The activity at the different vents are linked to distinct sources located at depths of 200–300 m NW of the crater terrace, as inferred from full-waveform, moment tensor inversion of the very-long-period (VLP; 0.05–0.5 Hz) explosive signals [*Chouet*, 2003; *Chouet et al.*, 2008]. The VLP source mechanism is attributed to the displacement of the magma flowing downward and around an expanding gas slug rising in the shallowest portion of the conduit system. At frequencies above the VLP band, the features of explosive signals likely result from the complex interplay between the turbulent dynamics of multiphase flow during the explosion, short-wavelength conduit vibrations, and the propagation of atmospheric pressure waves.

Throughout in the following, we investigate the broadband signals associated with the summit explosions in order to quantify the distributions of amplitude and recurrence times of explosive degassing at Stromboli Volcano.

4.1. Events Detection and Selection

A set of VLP events was detected using a method based on the STA/LTA approach [*Earle and Shearer*, 1994], calculated over signals band-pass filtered between 0.05 and 0.5 Hz. We applied this detection procedure to

recordings from the four summit stations shown in Figure 1, spanning the month of July 2011. To avoid local transients, we only accounted for events which were detected by at least three stations, thus obtaining a first catalogue amounting to 3407 detections.

We derived the polarization attributes (azimuth and incidence angles) by applying the method of *Kanasewich* [1981], which is based on the computation of the covariance matrix for the three components of ground motion. The elements of the covariance matrix are obtained from 30 s long windows of filtered signal from station STR6. The events azimuth angles measured clockwise from North vary in between 148° and 158° at station STR6 and ensure their association with the summit explosions. Over the VLP frequency band (0.05–0.5 Hz), the triggered events exhibit a high degree of waveform similarity, thus suggesting the action of a repetitive source mechanism. We thus repeated the matched filter procedure described above for a refined detection of events sharing similar waveforms, expecting that they are generated by the same source. First, we performed a correlation analysis over all the independent pairs of detections, using a 15 s long window encompassing the maximum amplitude of the 0.05–0.5 Hz filtered signal from summit station STR9 (see Figure 1). We then applied a clustering procedure, by grouping events whose correlation was greater than an arbitrary threshold equal to 0.8. In this manner, we identified two main VLP families, whose members were then aligned according to the interevent delay times derived from correlation analysis, and eventually stacked to derive a family representative template waveform. The matched filter processing is then iterated for the two different families, improving the catalogue (Family I: 2998 events; Family II: 1546 events). The overall final catalogue amounts to 4822 events containing the two families and 278 nonclassified events remaining from the catalogue obtained with the STA/LTA procedure. The two families present the same polarization attributes, with azimuth and incidence angles clustered over the 148°–158° and 75°–85° angular intervals, respectively. These results suggest that both groups of signals are caused by the same source. A simple projection of the wave vectors defined by the former polarization angles on a vertical section crossing the crater area indicates that the source is located at an elevation of about 600m asl (i.e., 150 m beneath the crater terrace), consistent with the results previously found by *Chouet* [2003] and *Chouet et al.* [2008]. From the above analysis, we inferred that the same seismic source generate signals of at least two different waveforms, which are likely representative of different explosive styles.

4.2. Amplitude and Interevent Times Distributions

Amplitudes over the VLP [0.05–0.5 Hz] and LP [0.3–2 Hz] frequency bands were computed by averaging the absolute-value seismograms over 22 s long and 10 s long time windows, respectively, centered at the largest peak-to-peak ground displacement.

These amplitudes are peaked at 0.5×10^{-6} m and 0.8×10^{-6} m for the LP and VLP bands, respectively (Figures 7a and 7b). The plot in Figure 7c illustrates that there is a general positive correlation between amplitudes computed over the VLP and LP frequency bands. The completeness of the catalogue has been determined through the information obtained with the families of similar events. We applied the detection test described above to both families of VLP events, determining a completeness threshold at 0.5×10^{-6} m. The associated threshold for the LP frequency band has been obtained by using the relationship between VLP and LP amplitudes. A VLP amplitude of 0.5×10^{-6} m corresponds to a LP amplitude varying between 0.29×10^{-6} m and 0.475×10^{-6} m (Figure 7c). We thus take the largest value of that range as a conservative estimate of LP amplitude threshold on catalogue completeness. Figure 8 shows the cumulative LP amplitude distribution of the explosive source with the completeness threshold set at 0.475×0^{-6} m. Again, we observe that the complete part of the catalogue (i.e., that part of the graph pertaining to amplitudes greater than the completeness threshold) is not fitted with a linear equation as would be expected for a typical GR distribution.

The distribution of interevent times is well described by a γ law (Figure 9), whose parameters ($\gamma = 1.52 \pm 0.09$ and $a = 0.62 \pm 0.04$ with a p value of 0.75 from a χ^2 test of the goodness of fit) are significantly different from those expected for tectonic activity (see equation (3)).

The probability density function of interevent times can also be fitted by a Weibull distribution given by

$$F(x;k,\lambda) = \frac{k}{\lambda}\left(\frac{x}{\lambda}\right)^{k-1} e^{(-x/\lambda)^k} \tag{4}$$

where λ and k are the scale and shape parameters, respectively, and the variable x represents the normalized inter-event times. The two parameters have been determined to be on the order of 1.03 and 1.26 (with a p value

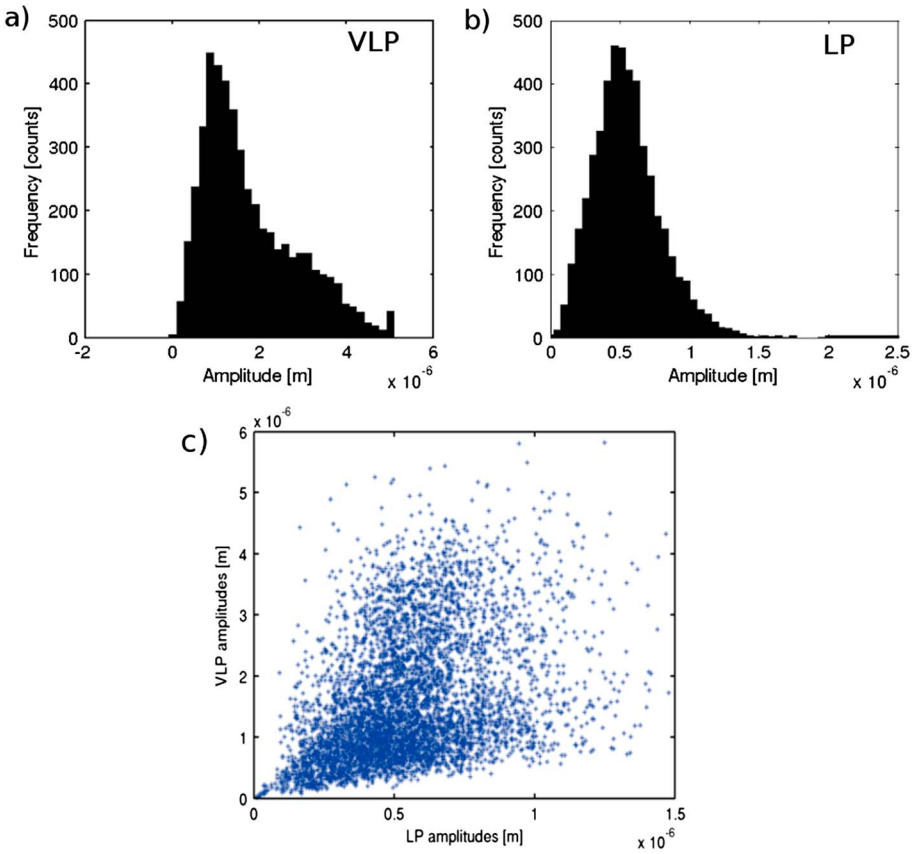

Figure 7. (a) Amplitude distribution of the events filtered between 0.05 and 0.5 Hz; (b) amplitude distribution of the events filtered between 0.3 and 2 Hz; (c) VLP amplitudes as a function of the LP amplitudes for the catalogue of the events related to the summit sources.

of 0.31 from application of χ^2 test). The shape parameter here obtained is close to that derived by *Taddeucci et al.* [2013] (*k* varying between 0.87 and 1.20) for the distribution of interexplosions times, as determined from the analysis of video recordings from a monitoring camera. This similarity thus brings additional support to the inferred one-to-one relationship between the VLP seismic records and the summit explosions.

The above results do highlight that the LP activity related to explosive degassing mechanism have a statistical behavior that deviate significantly from the laws which describe typical tectonic earthquake activity, both in terms of amplitude of interevent times distributions.

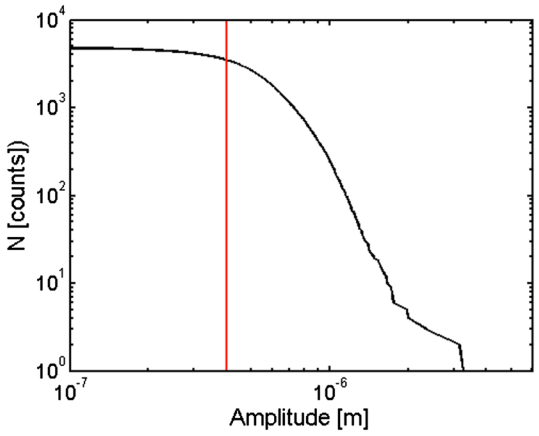

Figure 8. Cumulative LP amplitude distribution at Stromboli Volcano.

5. Statistical Test

In this section we compare the amplitude and recurrence time distributions for the complete parts of the catalogues obtained at Mount Etna and Stromboli Volcanoes. In order to relate events from two sources with different properties (size, location), the elements of the two different catalogues need to be reduced to a same scale by standardizing the amplitudes of the two data sets.

In particular, the two amplitude catalogues do not follow a Gaussian law, as they are truncated by the amplitude threshold. The use of the average and the standard deviation is therefore not

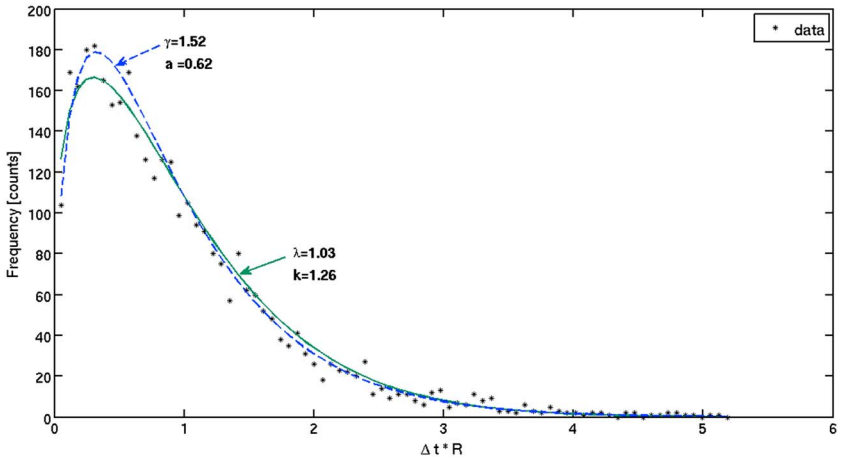

Figure 9. Interevent time distribution of LP events at Stromboli Volcano. The data (black dots) are fitted with a γ law (with parameters $\gamma = 1.52$ and $a = 0.62$—dashed line) and a Weibull distribution ($\gamma = 1.03$ and $k = 1.26$—continuous line). The Weibull distribution has been scaled on the x axis (with respect to equation (4)) in order to represent the results of the two fits on a same graph.

appropriate for the standardization of the distribution. We thus performed the standardization by (a) subtracting from individual amplitude bins the amplitude corresponding to the maximum of the distribution A_m and then by (b) dividing the distribution by the difference of the amplitude determined at half maximum of the distribution and A_m. The standardized distributions for Etna and Stromboli are represented in Figure 10a. We applied the Kolmogorov-Smirnov (KS) statistical test on the two distributions, which is defined as the maximum value of the absolute difference between two cumulative functions of the investigated data sets F_1 and F_2:

$$D_n = \mathrm{Sup_n}(|F_1(x) - F_2(x)|) \tag{5}$$

The null hypothesis that the two data sets are drawn from the same distribution is rejected at the $\alpha \cdot 100\%$ level if

$$D_n > \left[\frac{-1}{2}\left(\frac{1}{n_1} + \frac{1}{n_2}\right)\ln\left(\frac{\alpha}{2}\right)\right]^{0.5} \tag{6}$$

where n_1 and n_2 are the dimensions of the two compared data sets.

We obtained a KS statistic of 0.0226 against a critical value of 0.0283 which validates the hypothesis that the two data sets derive from the same distributions at the 95% confidence level (see Figure 10b).

At the same time, we also observed that the two data sets follow a similar behavior in terms of interevent times (Figure 11). Indeed, the KS test applied on the interevent times distributions scaled for the daily rates

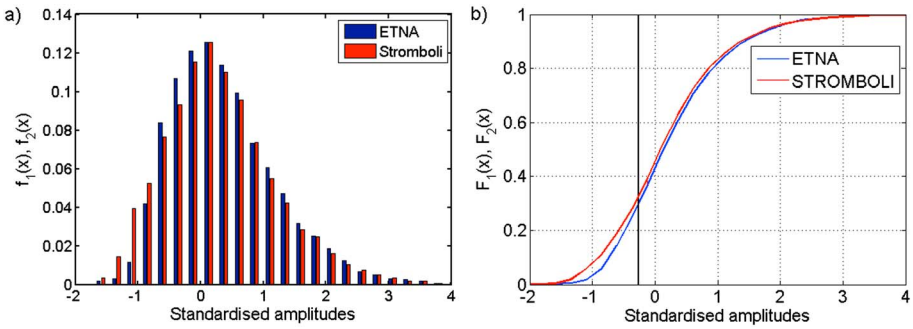

Figure 10. (a) Probability density distribution of the standardized amplitudes for the data sets of Etna (blue) and Stromboli (red); (b) associated cumulative distributions (F_1 and F_2), the black vertical line indicates the lower threshold considered in the KS test.

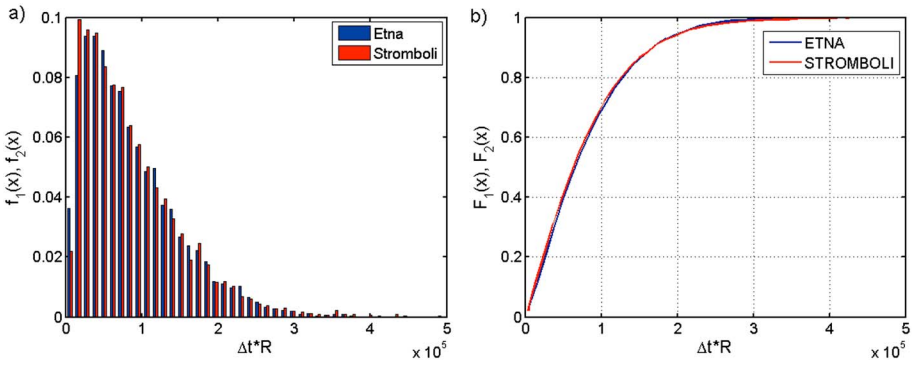

Figure 11. (left) Interevent times distributions of Mt Etna (f_1) and Stromboli (f_2). The distributions are normalized for the total number of events in the catalogues and scaled for the daily rates number of events. (right) Associated cumulative distributions of the two data sets F_1 and F_2.

of events (Stromboli: $R = 155$) demonstrates that the Stromboli and Etna interevent data are statistically indistinguishable at the 95% confidence level.

From these results, the generation of LP events at Mount Etna is likely driven by a degassing process, albeit at depth, statistically similar to the one driving the summit explosions at Stromboli Volcano.

6. Discussion and Conclusions

Over the past 30 years, the extensive observations of LP signals in volcanic/hydrothermal environments prompted numerous efforts aimed at unrevealing the mechanism of those sources. At present, however, a unique model able to explain the entirety of LP signals recorded in different contexts is still missing, mostly due to (i) difficulties in the robust and reliable estimate of the system of forces acting at the source and (ii) the frequent lack of evident surface manifestations associated with that class of signals. Following these obstacles, in this paper we attempted to constrain the source process of LP activity at Etna Volcano, Italy, from the detailed analysis of the statistics of a catalogue of events exhibiting similar waveforms. This catalogue was obtained from application of a matched filter procedure which fully exploits waveform similarity and the repetitive character of LP events. We assessed the completeness threshold of that catalogue from application of a new detection test, thus avoiding the effects due to the limitation in the detection procedures.

The complete component of the LP catalogue has been observed to differ significantly from the typical Gutenberg-Richter behavior commonly used for describing the amplitude distribution of tectonic earthquakes. *Bean et al.* [2014] reached the same conclusions analyzing data from Mount Etna and Turrialba Volcanoes. Using the damage mechanics model of *Amitrano* [2003], *Bean et al.* [2014] also demonstrated that their amplitude distributions are consistent with faulting in a weak and compliant medium, such as the volcanic upper edifice. Their attribution of the LP source process to a brittle failure mechanism was also supported by the observation of a relationship between the frequency and the size of the LP events.

In the present study, we also found that the γ law describing the LP interevent times is significantly different from that usually observed for tectonic activity, of a factor 0.5 in the shape parameter γ.

Similar analyses were conducted over a data set from Stromboli Volcano, for which the recorded VLP/LP transients are univocally associated with the recurrent summit explosions, characteristic of the Strombolian activity. Also in this case, we observed that the behavior of the seismicity associated with the explosive degassing process differs from the GR and the γ law usually expected in case of tectonic earthquakes: as for the Mount Etna case, the amplitudes are distributed according to a bell-shaped distribution, while the interevent times can be described by either a γ or a Weibull distribution, as previously derived by *Taddeucci et al.* [2013].

Statistical tests show that the Mount Etna LP activity behaves as the Strombolian explosive signals in terms of both amplitudes and interevent time distributions. The results from this study thus suggest that during the period under examination, LP activity at Mount Etna was likely driven by an intermittent degassing process, similar to that which is usually invoked to explain the summit explosions at Stromboli Volcano [i.e., *Blackburn et al.*, 1976].

However, there is a significant difference in terms of depth which is not understood: Etna's LP sources discussed above span the 300–1000 m depth interval (P1), which could explain the lack of any evident surface manifestation of the degassing process.

Regarding the establishment of an intermittent slug-flow regime evoked by *Blackburn et al*. [1976], this is usually explained as the consequence of bubble coalescence, which would in turn be controlled by either the relative flow velocities of the magma-gas mixture [e.g., *Parfitt*, 2004, and references therein] or geometrical complexities of the plumbing system [e.g., *Jaupart and Vergniolle*, 1988*; James et al*., 2004, 2006]. With the data presently available, it is impossible to distinguish which of these different, competing models is the most appropriate one for interpreting the discussed LP signals at Etna. Another possibility is that LP events at Etna are not direct indicators of the deeper degassing process but are a secondary effect caused by stress changes associated with degassing at depth (and hence mirror pulse-like degassing amplitude and interevent times statistics). This scenario would also be consistent with *Bean et al*. [2014]. To address these questions, the catalogue-driven approach would need to be applied over extended time series, encompassing periods of different volcanic activity [e.g., *De Martino et al*., 2011]. Furthermore, comparison with data from both lab experiments and numerical simulations of (i) brittle-fracturing of both low- and high-viscosity materials and (ii) fluid flow under different regimes is needed in order to better understand the physics governing the observed distributions. These steps should lead to an improved understanding of LP activity, in turn clarifying its significance in terms of eruption forecasting.

Acknowledgments
This study received funding from the Irish Research Council for Science, Engineering and Technology "Embark Initiative" and from the European Union 7th Framework Programme (FP7/2007-2013) project NEMOH, grant agreement 289976. The INGV department in Napoli is gratefully acknowledged for providing seismic data for both Etna and Stromboli Volcanoes.

References

Aki, K., M. Fehler, and S. Das (1977), Source mechanism of volcanic tremor: Fluid-driven crack models and their application to the Kilauea eruption, *J. Volcanol. Geotherm. Res.*, *2*, 259–287.

Amitrano, D. (2003), Brittle-ductile transition and associated seismicity: Experimental and numerical studies and relationships with the *b*-value, *J. Geophys. Res.*, *108*(B1), 2044, doi:10.1029/2001JB000680.

Arciniega-Ceballos, A., B. Chouet, and P. Dawson (2003), Long-period events and tremor at Popocatepetl volcano (1994–2000) and their broadband characteristics, *Bull. Volcanol.*, *65*(2), 124–135.

Aster, R., D. Zandomeneghi, S. Mah, S. McNamara, D. B. Henderson, H. Knox, and K. Jones (2008), Moment tensor inversion of very long period seismic signals from Strombolian eruptions of Erebus volcano, *J. Volcanol. Geotherm. Res.*, *177*(3), 635–647.

Bak, P., K. Christensen, L. Danon, and T. Scanlon (2002), Unified scaling law for earthquakes, *Phys. Rev. Lett.*, *88*(17), 178,501.

Bean, C. J., I. Lokmer, and G. Obrien (2008), Influence of near-surface volcanic structure on long-period seismic signals and on moment tensor inversions: Simulated examples from Mount Etna, *J. Geophys. Res.*, *113*, B08308, doi:10.1029/2007JB005468.

Bean, C. J., L. De Barros, I. Lokmer, J.-P. Métaxian, G. OBrien, and S. Murphy (2014), Long-period seismicity in the shallow volcanic edifice formed from slow-rupture earthquakes, *Nat. Geosci.*, *7*(1), 71–75.

Blackburn, E. A., L. Wilson, and R. J. Sparks (1976), Mechanisms and dynamics of Strombolian activity, *J. Geol. Soc.*, *132*(4), 429–440.

Cesca, S., J. Battaglia, T. Dahm, E. Tessmer, S. Heimann, and P. Okubo (2008), Effects of topography and crustal heterogeneities on the source estimation of LP event at Kilauea Volcano, *Geophys. J. Int.*, *172*(3), 1219–1236.

Chouet, B. (1985), Excitation of a buried magmatic pipe: A seismic source model for volcanic tremor, *J. Geophys. Res.*, *90*(B2), 1881–1893, doi:10.1029/JB090iB02p01881.

Chouet, B. (1986), Dynamics of a fluid-driven crack in three dimensions by the finite difference method, *J. Geophys. Res.*, *91*(B14), 13,967–13,992.

Chouet, B. (1988), Resonance of a fluid-driven crack: Radiation properties and implications for the source of long-period events and harmonic tremor, *J. Geophys. Res.*, *93*(B5), 4375–4400.

Chouet, B. (1992), A seismic model for the source of long-period events and harmonic tremor, in *Volcanic Seismology*, pp. 133–156, Springer, Berlin.

Chouet, B. (1996), New methods and future trends in seismological volcano monitoring, in *Monitoring and Mitigation of Volcano Hazards*, pp. 23–97, Springer, New York.

Chouet, B. (2003), Volcano seismology, *Pure Appl. Geophys.*, *160*(3), 739–788.

Chouet, B., G. Saccorotti, P. Dawson, M. Martini, R. Scarpa, G. De Luca, G. Milana, and M. Cattaneo (1999), Broadband measurements of the sources of explosions at Stromboli Volcano, Italy, *Geophys. Res. Lett.*, *26*(13), 1937–1940, doi:10.1029/1999GL900400.

Chouet, B., P. Dawson, T. Ohminato, M. Martini, G. Saccorotti, F. Guidicepietro, G. De Luca, G. Milana, and R. Scarpa (2003), Correction to "Source mechanisms of explosions at Stromboli Volcano, Italy, determined from moment-tensor inversions of very-long-period data," *J. Geophys. Res.*, *108*(B7), 2331, doi:10.1029/2003JB002535.

Chouet, B., P. Dawson, and M. Martini (2008), Shallow-conduit dynamics at Stromboli Volcano, Italy, imaged from waveform inversions, *Geol. Soc. London, Spec. Publ.*, *307*(1), 57–84.

Corral, A. (2003), Local distributions and rate fluctuations in a unified scaling law for earthquakes, *Phys. Rev. E*, *68*(3), 035102.

Corral, A. (2004), Long-term clustering, scaling, and universality in the temporal occurrence of earthquakes, *Phys. Rev. Lett.*, *92*(10), 108501.

Davi, R., G. S. O'Brien, I. Lokmer, C. J. Bean, P. Lesage, and M. M. Mora (2010), Moment tensor inversion of explosive long period events recorded on Arenal Volcano, Costa Rica, constrained by synthetic tests, *J. Volcanol. Geotherm. Res.*, *194*(4), 189–200.

De Barros, L., I. Lokmer, C. J. Bean, G. S. O'Brien, G. Saccorotti, J.-P. Métaxian, L. Zuccarello, and D. Patanè (2011), Source mechanism of long-period events recorded by a high-density seismic network during the 2008 eruption on Mt Etna, *J. Geophys. Res.*, *116*, B01304, doi:10.1029/2010JB007629.

De Martino, S., M. Falanga, M. Palo, P. Montalto, and D. Patanè (2011), Statistical analysis of the volcano seismicity during the 2007 crisis of Stromboli, Italy, *J. Geophys. Res.*, *116*, B09312, doi:10.1029/2010JB007503.

Earle, P. S., and P. M. Shearer (1994), Characterization of global seismograms using an automatic-picking algorithm, *Bull. Seismol. Soc. Am.*, *84*(2), 366–376.

Fujita, E., Y. Ida, and J. Oikawa (1995), Eigen oscillation of a fluid sphere and source mechanism of harmonic volcanic tremor, *J. Volcanol. Geotherm. Res.*, *69*, 365–378.

James, M. R., S. J. Lane, B. Chouet, and J. S. Gilbert (2004), Pressure changes associated with the ascent and bursting of gas slugs in liquid-filled vertical and inclined conduits, *J. Volcanol. Geotherm. Res.*, *129*, 61–82.
James, M. R., S. J. Lane, and B. A. Chouet (2006), Gas slug ascent through changes in conduit diameter: Laboratory insights into a volcano-seismic source process in low-viscosity magmas, *J. Geophys. Res.*, *111*, B05201, doi:10.1029/2005JB003718.
Jaupart, C., and S. Vergniolle (1988), Laboratory models of Hawaiian and Strombolian eruptions, *Nature*, *331*(6151), 58–60.
Kanasewich, E. R. (1981), *Time Sequence Analysis in Geophysics*, Univ. of Alberta, Edmonton, Alberta.
Kumagai, H., and B. A. Chouet (2001), The dependence of acoustic properties of a crack on the mode and geometry, *Geophys. Res. Lett.*, *28*, 3325–3328, doi:10.1029/2001GL013025.
Kumagai, H., B. A. Chouet, and M. Nakano (2002), Temporal evolution of a hydrothermal system in Kusatsu-Shirane Volcano, Japan, inferred from the complex frequencies of long-period events, *J. Geophys. Res.*, *107*(B10), 2236, doi:10.1029/2001JB000653.
Kumagai, H., B. A. Chouet, and P. B. Dawson (2005), Source process of a long-period event at Kilauea volcano, Hawaii, *Geophys. J. Int.*, *161*(1), 243–254.
Lokmer, I., C. J. Bean, G. Saccorotti, and D. Patane (2007), Moment-tensor inversion of LP events recorded on Etna in 2004 using constraints obtained from wave simulation tests, *Geophys. Res. Lett.*, *34*, L22316, doi:10.1029/2007GL031920.
Matoza, R. S., and B. A. Chouet (2010), Subevents of long-period seismicity: Implications for hydrothermal dynamics during the 2004–2008 eruption of Mount St. Helens, *J. Geophys. Res.*, *115*, B12206, doi:10.1029/2010JB007839.
Molchan, G. (2005), Interevent time distribution in seismicity: A theoretical approach, *Pure Appl. Geophys.*, *162*(6), 1135–1150.
Nakano, M., H. Kumagai, and B. A. Chouet (2003), Source mechanism of long-period events at Kusatsu-Shirane Volcano, Japan, inferred from waveform inversion of the effective excitation functions, *J. Volcanol. Geotherm. Res.*, *122*(3–4), 149–164.
Neuberg, J. (2000), Characteristics and causes of shallow seismicity in andesite volcanoes, *Philos. Trans. R. Soc., A*, *358*, 1533–1546.
Neuberg, J., and R. Luckett (1996), Seismo-volcanic sources on Stromboli Volcano, *Ann. Geophys.*, *39*(2), 377–391.
Neuberg, J., R. Luckett, M. Ripepe, and T. Braun (1994), Highlights from a seismic broadband array on Stromboli Volcano, *Geophys. Res. Lett.*, *21*(9), 749–752, doi:10.1029/94GL00377.
Neuberg, J., R. Luckett, B. Baptie, and K. Olsen (2000), Models of tremor and low-frequency earthquake swarms on Montserrat, *J. Volcanol. Geotherm. Res.*, *101*, 83–104.
Neuberg, J., H. Tuffen, L. Collie, D. Green, T. Powell, and D. Dingwell (2006), The trigger mechanism of low-frequency earthquakes on Montserrat, *J. Volcanol. Geotherm. Res.*, *153*(1), 37–50.
Parfitt, E. (2004), A discussion of the mechanisms of explosive basaltic eruptions, *J. Volcanol. Geotherm. Res.*, *134*, 77–107.
Ripepe, M., M. Rossi, and G. Saccorotti (1993), Image processing of explosive activity at Stromboli, *J. Volcanol. Geotherm. Res.*, *54*(3), 335–351.
Rosi, M., M. Pistolesi, A. Bertagnini, P. Landi, M. Pompilio, and A. Di Roberto (2013), Chapter 14 Stromboli Volcano, Aeolian Islands (Italy): Present eruptive activity and Hazards, *Geol. Soc. London, Mem.*, *37*, 473–490.
Shearer, P. M. (2009), *Introduction to Seismology*, Cambridge Univ. Press, Cambridge.
Taddeucci, J., D. M. Palladino, G. Sottili, D. Bernnini, D. Andronico, and A. Cristaldi (2013), Linked frequency and intensity of persistent volcanic activity at Stromboli (Italy), *Geophys. Res. Lett.*, *40*, 3384–3388, doi:10.1002/grl.50652.
Traversa, P., and J.-R. Grasso (2010), How is volcano seismicity different from tectonic seismicity?, *Bull. Seismol. Soc. Am.*, *100*, 1755–1769.
Tuffen, H., D. B. Dingwell, and H. Pinkerton (2003), Repeated fracture and healing of silicic magma generate flow banding and earthquakes?, *Geology*, *31*(12), 1089–1092.